communications physics

Article

https://doi.org/10.1038/s42005-024-01921-1

Pressure-sensitive in-situ underwater adhesives

Check for updates

Jiabin Liu, Parth Singh, Tsz Hung Wong & Shaoting Lin

While in-situ underwater adhesives are highly desirable for marine exploration and underwater robotics, existing underwater adhesives suffer from significantly reduced performance compared to air-cured adhesives, mainly due to difficulties in removing interfacial water molecules. Here, we develop a pressure-sensitive in-situ underwater adhesive featuring superabsorbent particles infused with functional silane and hydrogel precursors. When injected into an underwater crack, the particles quickly absorb water, swell, and fill the crack. Mechanical pressure is applied to improve particle-particle and particle-substrate interactions, while heat is utilized to trigger thermal polymerization of the hydrogel precursors. This process creates porous adhesives via bulk polymerization and forms covalent bonding with the substrate via surface silanization. Our experiments demonstrate that mechanical pressure significantly enhances the adhesive's stretchability (from 3 to 5), stiffness (from 37 kPa to 78 kPa), fracture toughness (from 1 kJ/m^2 to 7 kJ/m^2), and interfacial toughness with glass substrates (from 45 J/m^2 to 270 J/m^2).

Rapid and robust in-situ underwater adhesion is highly valuable for the exploration and utilization of underwater resources[1,2]. For offshore structures[3], such as subsea pipelines and ship hulls, returning damaged items to land for repair is often impractical, making underwater adhesion a critical component of the repair process. Furthermore, for marine robots[4] and underwater electronics[5], rapidly evacuating intruding water and achieving reliable adhesion on damaged components not only reduces economic losses but also prevents further damage. Despite its importance, achieving fast and reliable adhesion in an aqueous environment remains a fundamental challenge due to the presence of the hydration layer, a film of water molecules that forms between the adhesive and the wet substrates. This hydration layer hinders both molecular-scale chemical bonding and macro-scale physical contact between the adhesive and wet substrates, collectively reducing the overall adhesive strength[2,6].

Traditional underwater adhesives are typically categorized into two types: glue-based underwater adhesives that consist of liquid precursors, and tape-based underwater adhesives that consist of solid adherents. Glue-based underwater adhesives often employ mussel-inspired chemistry[7–12] to penetrate the hydration layer or incorporate hydrophobic monomers[13–15] to repel the hydration layer. Although these two approaches enable bonding directly with wet substrates, they face challenges in maintaining an adequate adhesion area as liquid precursors struggle to maintain intimate contact with wet surfaces. To address this, some glue-based adhesives incorporate hygroscopic components[16,17] to absorb the hydration layer, which remains technical challenging for achieving substantial water absorption. Additionally, most liquid precursors in glue-based underwater adhesives tend to spread and leak into the surrounding aqueous environment during the extended curing period, which significantly weaken their adhesive performance. In contrast, tape-based underwater adhesives focus on applying hydrophobic chemicals on the tape surface[18,19] or manufacturing microstructures at the tape surface[20–23] to repel the hydration layer and form physical bonds with wet surfaces. However, due to the nature of these physical bonds, tape-based underwater adhesives generally exhibit weaker adhesive strength. In summary, achieving an in-situ underwater adhesive with adhesive performance comparable to its counterparts cured in air remains a significant technical challenge but is highly desirable.

In this work, we develop a pressure-sensitive in-situ (PSIS) underwater adhesive consisting of three key components: superabsorbent particles, functional silane, and hydrogel precursors. The superabsorbent particles form a primary polymer network that rapidly and substantially absorbs interfacial water molecules[24]. The functional silane promotes adhesion by forming covalent bonds with wet substrates through surface silanization[25]. Simultaneously, the hydrogel precursors form a secondary polymer network that links superabsorbent particles while further strengthening individual particles through bulk polymerization[26–28]. Subsequently, we apply mechanical pressure prior to surface silanization and bulk polymerization, synergizing with the particles' osmotic pressure, to enhance particle-particle and particle-substrate contact. Our experiments show that applying mechanical pressure increases the adhesive area from 14% to 75% and reduces the bulk material's porosity from 82% to 25%. These factors contribute to significant improvements in the PSIS's bulk and adhesion properties, including stretchability from 3 to 5, modulus from 37 kPa to 78 kPa,

Department of Mechanical Engineering, Michigan State University, East Lansing, MI, USA. e-mail: linshaot@msu.edu

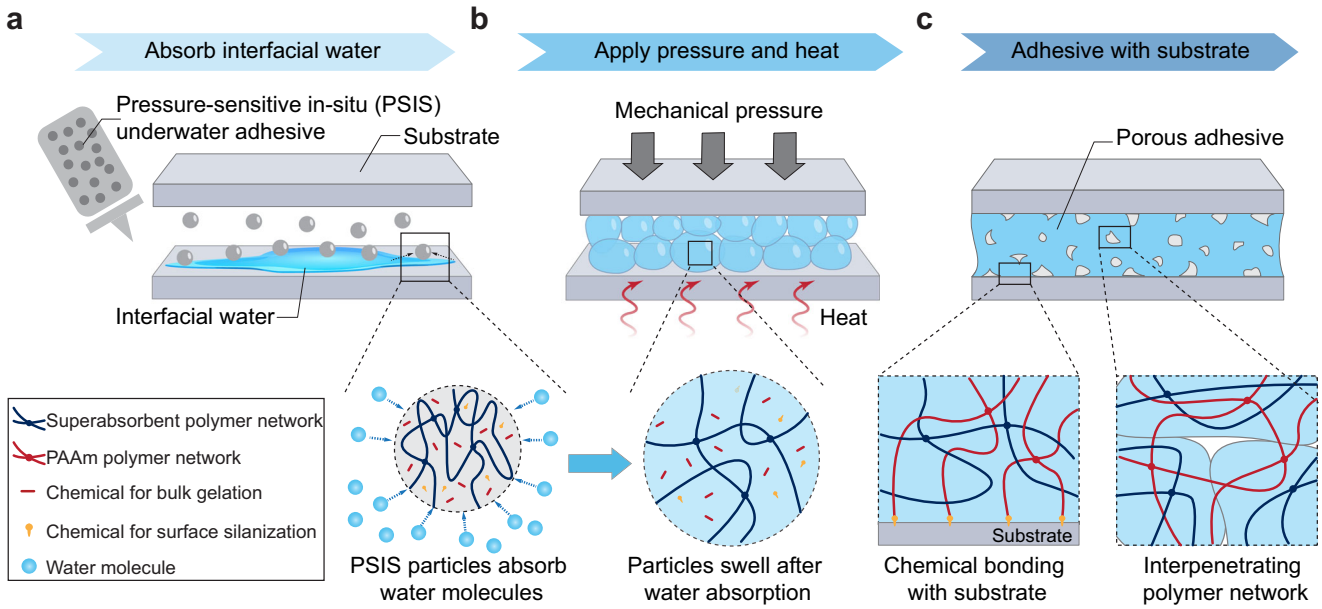


Fig. 1 | Working principle of pressure-sensitive in-situ underwater adhesion. **a** Schematic illustration of injecting pressure-sensitive in-situ (PSIS) underwater adhesive into a confined space containing interfacial water. The PSIS particles consist of superabsorbent polymeric particles, infused with chemicals for bulk gelation (i.e., acrylamide (AAm) monomer) and chemicals for surface silanization (i.e., 3-(trimethoxysilyl)propyl methacrylate (TMSPMA)). **b** After the PSIS particles absorb interfacial water, the particles swell to fill the confined space. Heat is applied for the thermal curing of the polyacrylamide (PAAm) polymer, while mechanical pressure is used to enhance the adhesive's bulk and interfacial toughness. **c** After curing, a bulk porous adhesive forms between the two substrates. The PAAm polymer chains form covalent bonds with the substrate, interpenetrate with the polymer network within the superabsorbent particles, and create connections between superabsorbent particles.

fracture toughness from 1 kJ m^{-2} to 7 kJ m^{-2}, and interfacial toughness with glass substrates from 45 J m^{-2} to 270 J m^{-2}. Notably, despite the PSIS's enhanced fracture and interfacial toughness, its hysteresis ratio slightly decreases with increasing mechanical pressure. Additionally, we investigate the effect of the amount of surrounding water molecules on the PSIS adhesive to understand its capability for evacuating interfacial water molecules. This work not only offers design strategies for rapid and tough in-situ underwater adhesive but also evokes mechanisms to enhance the adhesive's toughness without relying on a high hysteresis ratio.

Results and discussion

Working principle

Figure 1 illustrates the working principle of the pressure-sensitive in-situ (PSIS) underwater adhesive. The PSIS adhesive consists of superabsorbent particles embedded with functional silane and hydrogel precursors. Upon injection into an underwater crack, the PSIS adhesive rapidly absorbs and substantially stores the water molecules of the hydration layer due to the charged polymer chains within the superabsorbent particles[29,30] (Fig. 1a). Mechanical pressure is applied, synergizing with the particles' osmotic pressure, to further enhance the particle-particle and particle-substrate contacts (Fig. 1b). Concurrently, heat is utilized to initiate thermal polymerization of the hydrogel precursors. As illustrated in Fig. 1c, the combination of mechanical pressure and heat creates a porous adhesive via bulk polymerization while enabling covalent bonding between the adhesive and the substrate via surface silanization. Specifically, the functional silane in the PSIS adhesive covalently anchors long polymer chains (i.e., polyacrylamide polymers) to the substrate to create a robust adhesive bonding. Moreover, the hydrogel precursors in the PSIS adhesive form long-chain polymer networks that interconnect adjacent particles and interpenetrate with the primary polymer network within the superabsorbent particles, yielding a porous adhesive with superior stretchability and fracture toughness.

Swelling behavior of the PSIS particles

For an underwater adhesive capable of absorbing the hydration layer, the swelling speed and the water absorption capacity are two crucial parameters. To evaluate the swelling properties of PSIS particles, we measure the osmotic pressure of multiple PSIS particles in a water container. When the PSIS particles encounter interfacial water, the charged groups on the superabsorbent polymer chains attract the water molecules. This interaction creates a driving force, known as osmotic pressure, between the particle and the aqueous medium[31,32]. To measure the osmotic pressure, we first place a specific volume ratio φ_v of PSIS particles into a dry container with a porous cover (Fig. 2a), where φ_v is the volume ratio between the PSIS particles and the container. The porous cover has multiple penetrated holes that are designed to block particles from passing through while still allowing water molecules to flow freely. Next, we rapidly pour enough deionized water to fully submerge the container, while simultaneously recording the pressure required to keep the cover in place (Fig. 2a). Due to their tendency to absorb water, the particles continue to draw water molecules from the exterior to the interior until equilibrium is reached, where the internal osmotic pressure equals the externally applied pressure. Generally, as plotted in the Fig. 2b, the osmotic pressure gradually increases over time until it reaches a plateau, with its gradient decreasing progressively. When the volume of the particles is large (e.g., φ_v = 53%), the pressure increases rapidly in the initial 30 s and reaches a plateau of up to 8.5 kPa in around 70 s. In contrast, when the volume of the particles is small (e.g., φ_v = 12%), the particles need around 50 s to swell large enough to reach the porous cover, and the measured pressure increases slowly, reaching a plateau of 3 kPa in about 200 s. The sharp slope of the osmotic pressure Π versus time curve at t = 0~20 s of the PSIS particles with φ_v = 53% indicates a strong driving force for swelling. As the PSIS particles absorb water, the slope of the curve gradually diminishes, suggesting a reduction in the driving force for swelling as water absorption progresses. To further assess the swelling properties of PSIS particles, we capture sequential images of individual particle swelling freely in water under a light microscope[33] (Supplementary Fig. S1). The swelling ratio in diameter a/a_0 versus time t is plotted in Fig. 2c, where a represents the average swelling particle diameter and a_0 is the initial average diameter. The average diameter a is determined by calculating the square root of particle area captured in the focal plane. As shown in Fig. 2c, on average, the individual particles swell to ~3.5 times their initial diameter, which is approximately a 30-fold increase in volume. Additionally, the swelling ratio increases rapidly at the beginning and gradually reaches a plateau at around

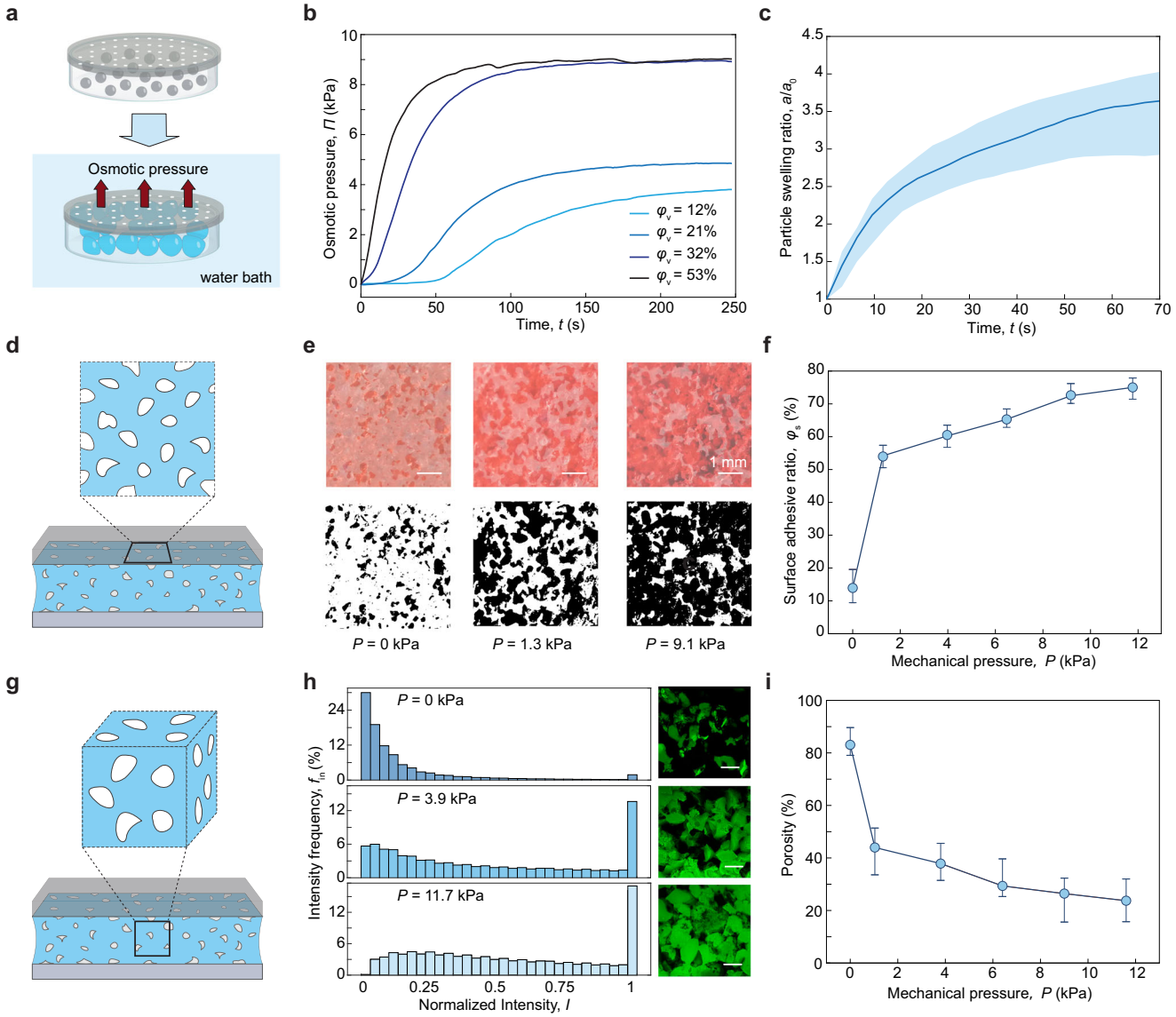


Fig. 2 | Swelling behavior of PSIS particles and structure characterizations of PSIS adhesives. a Schematic illustration of the osmotic pressure measurement of the particles of pressure-sensitive in-situ (PSIS) underwater adhesive. **b** Osmotic pressure Π versus time t for different volumes ratio φ_v of PSIS adhesive particles. φ_v is the volume ratio between the PSIS particles and the container. **c** The swelling ratio in diameter a/a_0 of individual PSIS particle versus time. a represents the average diameter of swelling particles and a_0 is the initial average diameter of particles. Values represent the mean ± s.d. ($N = 7$). **d** Schematic illustration of the bulk PSIS adhesive contacts with the substrate. The blue area represents the adhesive region, while the white area represents voids. **e** The upper images show the bulk PSIS adhesive in contact with glass slides, and the lower images show the processed results, where the black region represents the adhesive area, and the white region represents the void area. The scale bar is 1 mm. **f** The surface adhesive ratio φ_s increases with the applied mechanical pressure P.Values represent the mean ± s.d. ($N = 3$). **g** Schematic illustration of the porous PSIS adhesive. The blue area represents the material, while the white area represents voids. **h** 3D images of the PSIS adhesive material and the corresponding histograms showing the relationship between intensity frequency f_{in} and intensity I. The scale bar is 400 μm. **i** The porosity of the PSIS adhesive decreases with applied mechanical pressure P. Values represent the mean ± s.d. ($N = 3$).

70 s. Combined with the osmotic pressure experiments, these results indicate that PSIS particles exhibit substantial water absorption capacity along with a fast swelling speed, making it highly effective for evacuating large amounts of water in underwater adhesion applications.

Structure characterization of the PSIS adhesive

To characterize the ability of mechanical pressure to enhance particle-particle and particle-substrate contacts, we examine two key factors: the contact area between adhesive and substrate (Fig. 2d) and the porosity of the adhesive material, both of which affect the adhesive's bulk and adhesive properties. To investigate the impact of mechanical pressure on these two factors, we synthesize the bulk material upon transparent glass slides under controlled mechanical pressure, ranging from 0 to 12 kPa. We capture images of the adhesive surface under white light to quantitively analyze the adhesive area between the bulk material and the substrate (Supplementary Fig. S2). The distinct color differences between the air gap and the adhesive area—white for the air gap and red for the adhesive—allow us to clearly distinguish the adhesive area in the captured images. Figure 2e shows the captured images with their processed results, where the black region represents the adhesive area, and the white region represents the void area. As mechanical pressure increases, the processed results shift from being dominated by white (i.e., void area) to black (i.e., adhesive area), indicating that the adhesive area significantly increases with applied pressure. As summarized in Fig. 2f, the surface adhesion ratio φ_s, defined as the ratio of the adhesive area to the total area, increases from 14% to 75% as mechanical pressure increases. During bulk polymerization, the increased contact area

with the substrate provides more chances for polymer chains to chemically anchor to the substrate, thereby enhancing intrinsic adhesion toughness and improving overall adhesion performance.

Mechanical pressure impacts not only the contact between the adhesive and substrate but also the internal structure of the porous adhesive material, particularly its porosity, defined as the ratio of void volume to total volume (Fig. 2g). Generally, higher porosity results in lower stiffness and decreased toughness since the void spaces reduce the load-bearing area of the material[34]. To determine the porosity of the adhesive material, we scan the bulk material mixed with fluorescent tracers at a constant area (i.e., 3600 μm × 2700 μm) in the depth direction, taking measurements every 5 μm for a total 200 μm depth. Supplementary Fig. S3 shows the confocal images of the PSIS adhesive captured at different focal depths. We then sum the pixel intensity across all scanned depths and determine the porosity by calculating the ratio of the number of pixels with low intensity (e.g., $I < 0.2$) to the total number of pixels. Figure 2h illustrates 3D volumetric images of PSIS adhesive, which is constructed from a spatial sequence of 2D images scanned across different depth, depicting the microscopic-scale PSIS adhesive formed under various mechanical pressures. Additionally, corresponding histograms are provided, illustrating the relationship between intensity frequency f_{in} versus intensity I. For the PSIS adhesive formed without pressure (i.e., $P = 0$ kPa), the material consists of dispersed particles with large void space, and its histogram is primarily concentrated at low intensity (i.e., $I = 0$). In contrast, for the PSIS adhesive formed under high pressure (i.e., $P = 11.7$ kPa), the material consists of densely packed particles with small void space, and its histogram is primarily concentrated at high intensity (i.e., $I = 1$). As summarized in Fig. 2i, the porosity of the bulk PSIS adhesive decreases from 82% to 25% as the applied mechanical pressure increases.

Bulk performance of the PSIS adhesive

We next investigate the impact of the applied mechanical pressure on the bulk performance of the PSIS adhesive. First, we conduct uniaxial tensile tests (Fig. 3a) to measure the relationship between nominal stress S and stretch ratio λ of the PSIS adhesives formed under various mechanical pressures P. As shown in Fig. 3b, as the mechanical pressure increases, the stretchability rises from 3 to 5, while the shear modulus increases from 37 to 78 kPa (Supplementary Fig. S4). This is because the strengthened connection between particles, resulting from mechanical pressure, improves the material's stretchability. Additionally, as the applied pressure increases, the bulk PSIS adhesive exhibits lower porosity, indicating a higher polymer density per volume, leading to increased stiffness. Next, we perform cyclic loading-unloading tensile tests on the materials at increasing stretch ratios (Supplementary Fig. S5). The corresponding hysteresis versus stretch ratios are summarized in Fig. 3c. As the stretch ratio increases, the hysteresis consistently rises. Notably, the hysteresis of the material formed under high pressure (i.e., $P = 11.7$ kPa) is lower than that of the material formed under low pressure (i.e., $P = 1.3$ kPa) at the same stretch ratios. Unlike traditional tough hydrogels that rely on high hysteresis for toughness enhancement[2,26,35], the PSIS adhesive exhibits enhanced toughness without relying on a large hysteresis ratio. As the loading force increases, the void space inside the material enlarges, causing the hysteresis ratio to increase with the stretch ratio. Moreover, materials formed under higher mechanical pressure exhibit lower porosity and stronger bonding in the connected areas, which allows them to bear tensile force more effectively, resulting in lower hysteresis when subjected to cyclic loading.

To assess the PSIS adhesive's fracture toughness, which characterizes its ability to resist crack propagation under a single cycle of loading, we first conduct pure-shear tensile tests to measure the nominal stress versus stretch ratio of an unnotched sample (Supplementary Fig. S6). Subsequently, we perform pure-shear tensile tests on a notched sample to determine the critical stretch λ_c, which is defined as the stretch ratio before crack propagation. As shown in Fig. 3d, the solid material around the crack tip undergoes significant deformation to prevent crack propagation during tensile loading. Given the measured critical stretch λ_c, the fracture toughness can be determined using the equation $\Gamma = H\int_1^{\lambda_c} S d\lambda$, where H is the initial length of the sample, and S and λ are the nominal stress and the stretch ratio applied on the unnotched sample. As summarized in Fig. 3e, f, with the increase in mechanical pressure, the critical stretch ratio is enhanced from 2.9 to 4.6, corresponding to a significant improvement in fracture toughness from 1 kJ m^{-2} to 7 kJ m^{-2}. The high fracture toughness achieved in the PSIS adhesive can be attributed to two factors: the molecular design within the PSIS particles and the structural alternation induced by the mechanical pressure. When we prepare the PSIS particles, a hydrogel precursor with a high monomer concentration (water-to-monomer ratio of 5.7) is used, resulting in a densely entangled long-chain polymer network within the adhesive. These long polymer chains collectively distribute the applied load by sliding through molecular entanglements without breaking, thereby enhancing crack propagation resistance and significantly improving the material's fracture toughness. In addition, the enhancement in fracture toughness due to mechanical pressure is mainly attributed to two factors: the reduced porosity of the bulk PSIS adhesive and the increased bonding strength between neighboring particles. Specifically, for the PSIS adhesive under high mechanical pressure, its porosity is reduced, leading to smaller void spaces that increase the load-bearing area, allowing the material to withstand greater mechanical stress. Additionally, the application of mechanical pressure during bulk polymerization creates stronger bondings between particles, further enhancing the material's resistance to fracture. These two factors collectively enhance the material's ability to resist crack propagation, resulting in an increased fracture toughness with mechanical pressure. We also test the feasibility of fabricating PSIS adhesive using UV initiation. The fracture toughness of the PSIS adhesive fabricated with the photoinitiator increases from 2 kJ m^{-2} to 5 kJ m^{-2} as the mechanical pressure increases from 1.3 to 9.1 kPa (Supplementary Fig. S7). The choice between thermal and UV initiation depends on the specific application requirements. For example, UV initiation is suitable for optically transparent substrates with low thermal conductivity, whereas thermal initiation is more appropriate for optically opaque substrates with high thermal conductivity.

We further investigate the effect of surrounding water molecules on the PSIS adhesive to understand its capability for evacuating interfacial water molecules. Specifically, we inject PSIS particles into a confined space with various water absorption ratios φ_w (the ratio of the volume of interfacial water divided by the volume of PSIS particles), from 0% to 100%, and then apply mechanical pressure ($P = 11.7$ kPa) to synthesize the bulk PSIS adhesive (Fig. 3g). As φ_w increases, the average particle diameter gradually increases from 1.2 mm to 1.9 mm (Supplementary Fig. S8). We first compare the pressure-dependent toughness enhancement of the PSIS adhesive with and without water absorptions. As shown in Fig. 3f, similar to the PSIS adhesive without water absorption $\varphi_w = 0\%$, the fracture toughness of the PSIS with $\varphi_w = 20\%$ improves significantly from 50 J m^{-2} to 4 kJ m^{-2} as the mechanical pressure increases. We further investigate the effect of surrounding water molecules on the modulus and toughness of the PSIS adhesive. As summarized in Fig. 3h, i, the shear modulus of the bulk material decreases from 78 kPa to 15 kPa, with the fracture toughness decreases from 7 kJ m^{-2} to 0.2 kJ m^{-2}. The reduction in stiffness and toughness can be attributed to two primary factors. First, upon absorbing water, the particles become softer and more brittle, reducing their ability to withstand mechanical stress. Second, water absorption decreases the density of long-chain polymers, resulting in weaker bonding between particles. Therefore, the material's ability to resist crack propagation decreases as the PSIS absorbs interfacial water molecules. In practical applications, PSIS particles will be rapidly injected into a confined space, leading to the absorption of a limited amount of water rather than free swelling, thus preserving good mechanical performance (Supplementary Fig. S9). In our future work, we will develop an integrated device capable of injecting PSIS particles, applying mechanical pressure, and supplying heat for use in underwater adhesion applications.

Adhesive performance of the PSIS adhesive

To further investigate the impact of mechanical pressure on the adhesion performance of the PSIS adhesive, we carry out standard 90° peeling tests (Supplementary Fig. S10) at a peeling rate of 0.5 mm s^{-1} to measure the

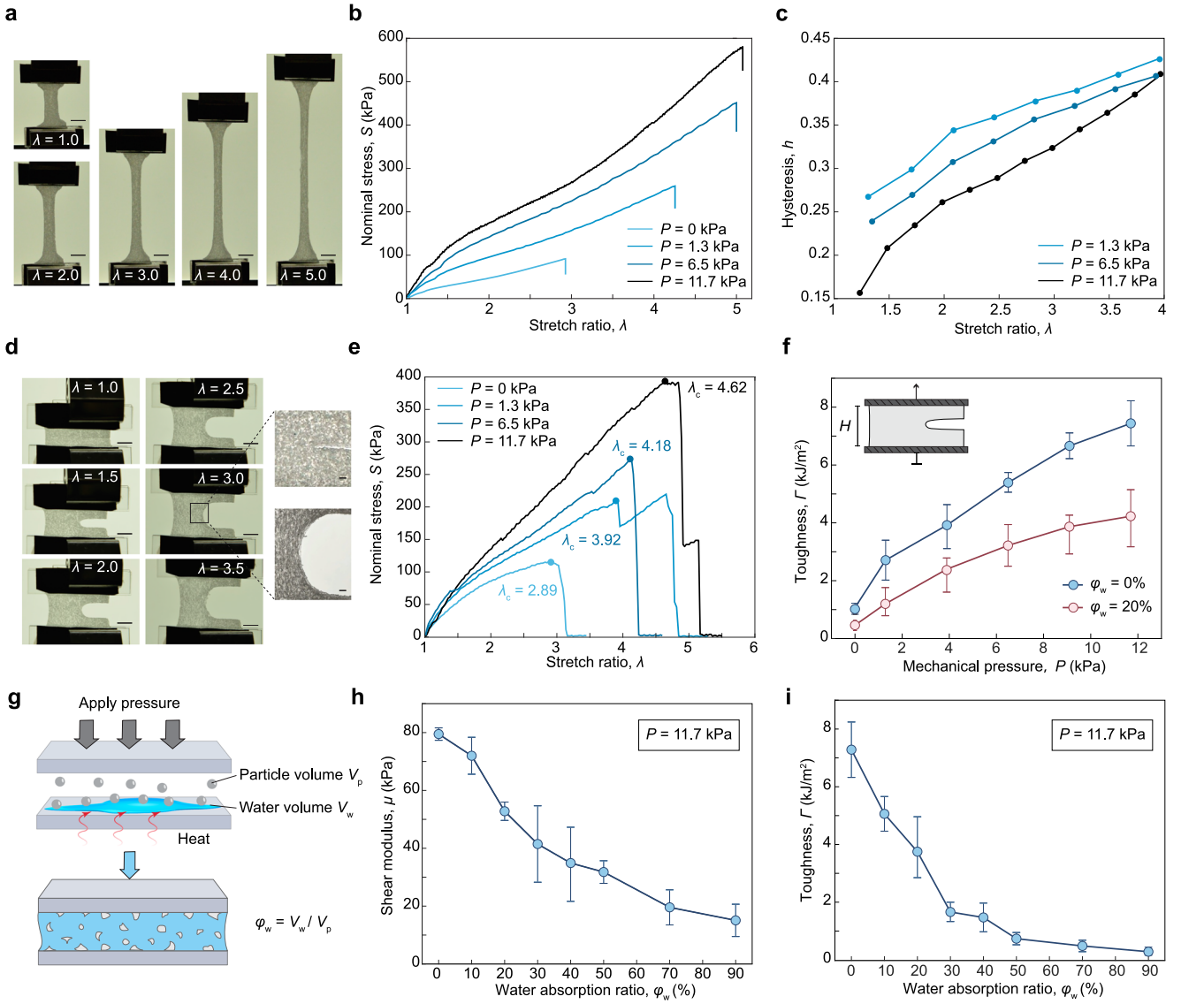


Fig. 3 | Bulk characterization of the pressure-sensitive in-situ underwater adhesive. a Images of the dog-bone-shaped pressure-sensitive in-situ underwater (PSIS) adhesive under uniaxial tension. The scale bar is 10 mm. **b** The measured nominal stress S versus stretch ratio λ of the PSIS adhesive synthesized under various mechanical pressures P. **c** The measured hysteresis h versus stretch ratio λ of the PSIS adhesive synthesized under various mechanical pressures P. **d** Images of a notched PSIS adhesive under pure shear tensile test. The scale bar is 10 mm. **e** Nominal stress S versus stretch ratio λ of notched PSIS adhesive synthesized under various mechanical pressures P. The highest point of each curve determines the critical stretch ratio λ_c, at which the crack propagates. **f** The fracture toughness Γ increases with the mechanical pressure P. Values represent the mean ± s.d. ($N = 3$). **g** Schematic illustrates the volume of PSIS adhesive particles and interfacial water. V_p represents the volume of PSIS particles, V_w represents the volume of interfacial water, and φ_w represents the water absorption ratio. **h** The shear modulus μ of adhesive decreases with the increase of water absorption ratio φ_w. Values represent the mean ± s.d. ($N = 3$). **i** The measured fracture toughness Γ decreases with the increase of water absorption φ_w. Values represent the mean ± s.d. ($N = 3$).

interfacial toughness between the adhesive material with glass substrates. As illustrated in Fig. 4a, a thin transparent nylon film is attached to the adhesive material to prevent it from stretching along the peeling direction. As the peeling force increases, the material around the interfacial crack front is significantly deformed. After the peeling force reaches a critical value, the crack starts to propagate along the adhesive surface. The interfacial toughness Γ_{in} is defined as the average peeling force F at steady state divided by the width W of adhesive material. From the peeling process, the measured interfacial toughness Γ_{in} is contributed by two parts: the intrinsic work of adhesion Γ_0 resulting from the scission of anchored polymer chains, and the dissipation energy Γ_D arising from material deformation[25]. Figure 4b presents the curves of peeling force per unit width versus the peeling displacement of adhesive materials formed under various mechanical pressures. As summarized in Fig. 4c, the interfacial toughness increased from 45 J m^{-2} to 270 J m^{-2} with the application of mechanical pressure P. For the PSIS adhesive material without absorbing interfacial water, its failure occurs at the adhesive surface, known as adhesive failure, primarily attributed to the scission of anchored polymer chains. As mechanical pressure increases, the adhesive area between the material and substrate increases, leading to a significant improvement in the intrinsic adhesion toughness.

Furthermore, we conduct 90° peeling tests on the PSIS adhesives that absorb varying amounts of water, with φ_w ranging from 0% to 80%, under a constant mechanical pressure ($P = 11.7$ kPa) to investigate the impact of surrounding water molecules on adhesive performance of the PSIS adhesive. As depicted in the molecular schematics in Fig. 4d, for PSIS adhesive with low water absorption ratio (i.e., $\varphi_w = 10\%$), the adhesive exhibits higher bulk strength compared to adhesion strength, leading to adhesive failure at the interface between PSIS adhesive and the solid substrate. During peeling test, the adhesive detaches from the solid surface, indicating a breakage of the polymer chains anchored to the solid substrate. In contrast, for PSIS

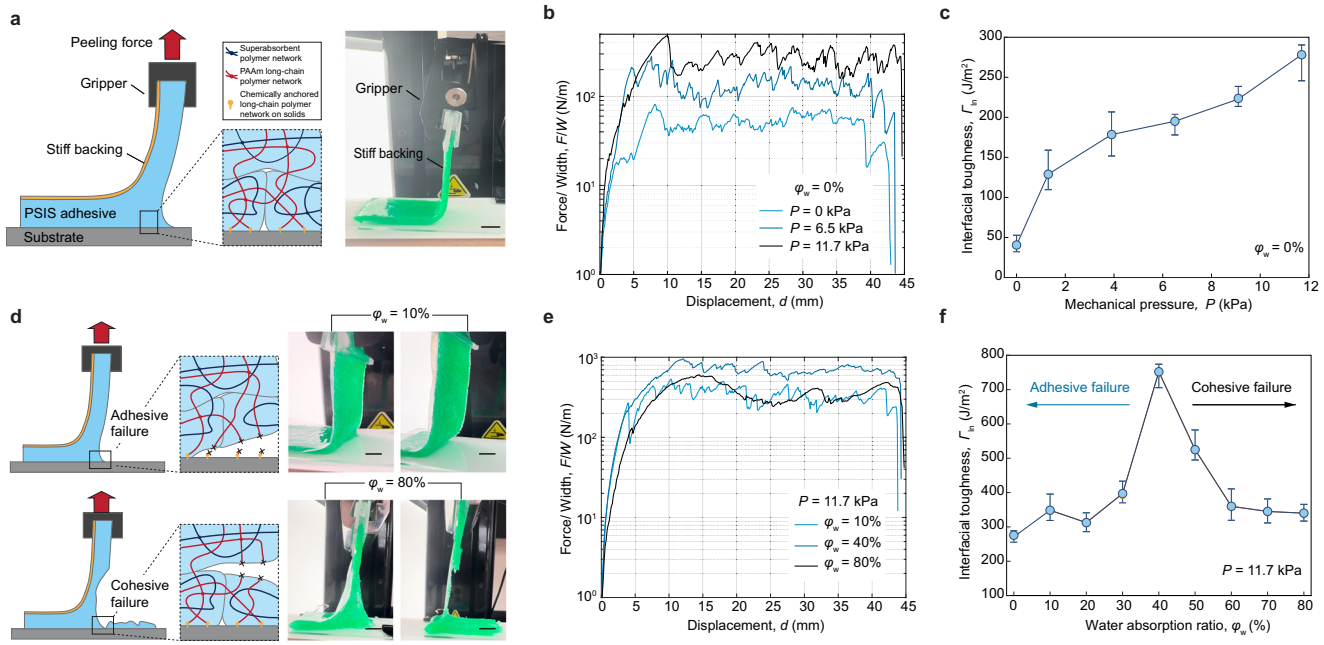


Fig. 4 | Adhesion characterization of the pressure-sensitive in-situ underwater adhesive. a Schematic and image of the pressure-sensitive in-situ underwater (PSIS) adhesive attached to a glass substrate prior to the 90-degree peeling test. The stiff backing is adhered to the back of the bulk PSIS adhesive. The scale bar is 10 mm. **b** The measured peeling force over width F/W versus displacement d of the PSIS adhesive synthesized under various mechanical pressures P. **c** The interfacial toughness Γ_{in} increases with the applied mechanical pressure P. Values represent the mean ± s.d. ($N = 3$). **d** Schematics and images represent adhesive failure and cohesive failure of the PSIS adhesives with low and high water absorption ratios φ_w. The scale bar is 10 mm. **e** The measured peeling force over width F/W versus displacement d of the PSIS adhesive with different water absorption ratio φ_w. **f** The measured interfacial toughness Γ_{in} versus water absorption ratio φ_w. As the water absorption ratio increases, the peeling failure mode changes from adhesive failure to cohesive failure.

adhesive with high water absorption ratio (i.e., $\varphi_w = 80\%$) in Fig. 4d, the adhesive exhibits lower bulk strength compared to adhesion strength, leading to cohesive failure within the bulk material. As the peeling force increases, the interfacial crack starts to kink and propagate through the bulk PSIS adhesive, resulting in residual adhesive material remaining on the substrate. As more water is absorbed, the failure mode transitions from adhesive failure to cohesive failure. Figure 4e presents the curves of peeling force per unit width versus the peeling displacement of adhesive materials formed with various water absorption ratios. Additionally, the corresponding interfacial toughness, as summarized in Fig. 4f, exhibits a non-monotonic trend, initially increasing and then decreasing. Since the intrinsic work of adhesion is correlated with the contact area between the adhesive and the substrate, we conducted experiments to measure the surface adhesion ratio φ_s under the same mechanical pressure (i.e., $P = 11.7$ kPa) but with different water absorption ratios φ_w (Supplementary Fig. S11). As the water absorption ratio increases, the contact area between the glass slides and the PSIS adhesive exhibit a non-monotonic trend, which initially increases and then slightly decreases. This occurs because, as the PSIS particles absorb water, they have a stronger driving force to interact with the substrate and the particle become softer, resulting in enhanced contact under mechanical pressure. However, when the particles absorb excessive water, such as at $\varphi_w = 80\%$, their size increases significantly, creating larger gaps between them, leading to a slight reduction in the contact area. For PSIS adhesives with a low water absorption ratio, inadequate contact with the substrate results in low adhesive strength, despite the material having high toughness. This combination leads to adhesive failure. In this case, the intrinsic adhesion energy governs the interfacial toughness. For the PSIS adhesive with a high-water absorption ratio, the PSIS particles can swell sufficiently to fully contact the substrate, leading to enhanced adhesion strength. However, due to the large swelling ratio, the bulk PSIS adhesive material becomes significantly weaker, resulting in cohesive failure with low interfacial toughness. For the PSIS adhesive with moderate water absorption ratios (i.e., $\varphi_w = 40\%$), both the scission of anchored polymer chains and the dissipation energy within the material synergistically contribute to the interfacial toughness, resulting in a high interfacial toughness (~750 J m^{-2}). The non-monotonic dependence of interfacial toughness on the amount of interfacial water molecules highlights the importance of controlling the water content to be absorbed by the PSIS adhesive in practical applications, an aspect that will be further explored in future studies. To evaluate the practical application of our PSIS as an underwater adhesive, we build a customized experiment setup to demonstrate its performance in real settings. We compare the lap shear test results of a sample formed in air under a mechanical pressure of 10 kPa with a sample cured underwater formed at an injection rate of 0.5 mL s^{-1}. The adhesive strength of the underwater sample is slightly lower than that of the in-air sample, which is due to the swelling of PSIS particle by absorbing water molecules (Supplementary Fig. S12).

Conclusion

In this paper, we present a pressure-sensitive in-situ (PSIS) underwater adhesive capable of absorbing large amounts of water and rapidly forming covalent chemical bonds with substrates in an aqueous environment. This PSIS adhesive consists of granular superabsorbent polymeric particles infused with functional silane and hydrogel precursor. Our experiments demonstrate that the PSIS particles have superior swelling capacity with a fast-swelling speed, which can absorb water 30 times their volume in 70 s. Moreover, we experimentally investigate the impact of mechanical pressure on the adhesive material's structure and find that the contact area between the adhesive and substrate increases from 14% to 75%, while the porosity of the adhesive material decreases from 82% to 25%. Furthermore, the adhesive material's stretchability, stiffness, and toughness are significantly enhanced by the application of mechanical pressure. This is because the mechanical pressure not only removes void spaces between particles, but also allows the long-chain polymers to form robust connections at the contact area between particles. Moreover, through 90° peeling experiments, we find that the interfacial toughness is improved by mechanical pressure, from 45 J m^{-2} to 270 J m^{-2}. Additionally, we study the impact of absorbed water on the mechanical properties and adhesive performance. The experiments demonstrate that a low water absorption ratio results in

inadequate substrate contact, leading to adhesive failure, while high absorption reduces the material's modulus and toughness, causing cohesive failure. Overall, we propose a design strategy for an adhesive capable of achieving in-situ adhesion under underwater conditions. In the future, we will further evaluate the material properties and adhesive performance under confined aqueous environments, discuss the impact of salt concentration, and address long-term durability issues of this PSIS adhesive.

Methods

Materials

Unless otherwise specified, the chemicals used in this work were used without further purification. The granular sodium polyacrylate homopolymers (Superabsorbent Polymer, Waste Lock 770) were purchased from M2 Polymer Technologies. Acrylamide (AAm, Sigma-Aldrich A8887), ammonium persulfate (APS, Sigma-Aldrich A3678), N,N,N',N'-tetramethylethylenediamine (TEMED, Sigma-Aldrich T9281), acetic acid (Sigma-Aldrich A6283), 3-(trimethoxysilyl)propyl methacrylate (TMSPMA; Sigma-Aldrich 440159) used in this work were purchased from Sigma-Aldrich. The plain microscope slides for 90° peeling tests and contact area measurement used in this work were purchased from Corning.

Synthesis of the PSIS particles

To synthesize the PSIS particles, we first prepared the silane solution for surface silanization. The silane solution was prepared by magnetic stirring (500 rpm) a mixture of 200 mL deionized water, 30 μL acetic acid, and 800 μL TMSPMA for 5 h until the mixture became transparent. For the long-chain polyacrylamide (PAAm) polymer network, acrylamide (AAm) was used as the monomer, TMSPMA in the silane solution served as the crosslinker, ammonium persulfate (APS) as the thermal initiator, and TEMED as the crosslinking accelerator. To prepare the pre-gel solution, we dissolved 3.5 g of AAm monomer in 5 mL of the silane solution followed by the addition of 170 μL of 0.1 M APS solution and 7 μL of TEMED to prepare the pre-gel solution of PAAm-hydrogel. The mixture was vortexed for 1 min. Then, we added 1.5 g of granular superabsorbent particles into the pre-gel solution and vortexed for 1 min until it evenly absorbed the AAm pre-gel solution. The PSIS particles were stored in a 5 °C refrigerator before use.

Synthesis of the PSIS adhesive

To synthesize PSIS adhesive with varying amounts of interfacial water (1 mL to 10 mL) for mechanical tests, we first added varying amounts of deionized water into a poly bag (75 mm × 50 mm), followed by 10 g of PSIS particles. The poly bag was then sealed using its zip closure, and the particles were left inside the bag for 10 s to allow the particles to absorb the water. For each sample, we used a needle with a diameter of 0.7 mm to create ~100 holes evenly on the surface of each bag. These holes were used to expel excess air when applying mechanical pressure. Subsequently, we placed each sample on a hotplate at 80 °C and used a universal testing machine (CellScale Testing Machine) to apply compression forces of 5 N, 15 N, 25 N, 35 N, and 45 N evenly on them, respectively, for 10 min until thermal curing.

Data availability

The data supporting the plots within the main text are available in Supplementary Data. Additionally, the original and processed datasets on swelling behaviors of PSIS particles and mechanical and structural characterizations of PSIS adhesives have been made publicly accessible via the public repository figshare (https://figshare.com) and are available here: https://doi.org/10.6084/m9.figshare.28013078. Further information is available from the corresponding author upon reasonable request.

Received: 11 September 2024; Accepted: 19 December 2024;
Published online: 02 January 2025

References

1. Fan, H. Getting glued in the sea. *Polym. J.* **55**, 653–664 (2023).
2. Fan, H. & Gong, J. P. Bioinspired underwater adhesives. *Adv. Mater.* **33**, 2102983 (2021).
3. Momber, A., Plagemann, P. & Stenzel, V. The adhesion of corrosion protection coating systems for offshore wind power constructions after three years under offshore exposure. *Int. J. Adhes. Adhes.* **65**, 96–101 (2016).
4. Zereik, E., Bibuli, M., Mišković, N., Ridao, P. & Pascoal, A. Challenges and future trends in marine robotics. *Annu. Rev. Control* **46**, 350–368 (2018).
5. Cao, Y. et al. Self-healing electronic skins for aquatic environments. *Nat. Electron.* **2**, 75–82 (2019).
6. Ma, X. et al. Hydrogels for underwater adhesion: adhesion mechanism, design strategies and applications. *J. Mater. Chem. A* **10**, 11823–11853 (2022).
7. North, M. A., Del Grosso, C. A. & Wilker, J. J. High strength underwater bonding with polymer mimics of mussel adhesive proteins. *ACS Appl. Mater. Interfaces* **9**, 7866–7872 (2017).
8. Ahn, B. K. Perspectives on mussel-inspired wet adhesion. *J. Am. Chem. Soc.* **139**, 10166–10171 (2017).
9. Cholewinski, A., Yang, F. K. & Zhao, B. Algae–mussel-inspired hydrogel composite glue for underwater bonding. *Mater. Horiz.* **6**, 285–293 (2019).
10. Lee, B. P., Messersmith, P. B., Israelachvili, J. N. & Waite, J. H. Mussel-inspired adhesives and coatings. *Annu. Rev. Mater. Res.* **41**, 99–132 (2011).
11. Lee, H., Dellatore, S. M., Miller, W. M. & Messersmith, P. B. Mussel-inspired surface chemistry for multifunctional coatings. *Science* **318**, 426–430 (2007).
12. He, S. et al. Bio-inspired instant underwater adhesive hydrogel sensors. *ACS Appl. Mater. Interfaces* **14**, 45869–45879 (2022).
13. Zhou, J. et al. Epoxy adhesive with high underwater adhesion and stability based on low viscosity modified Mannich bases. *J. Appl. Polym. Sci.* **135**, 45688 (2018).
14. Dolez, P., Williams, C., Goff, A. & Love, B. Properties of photopolymerisable acrylic adhesives for underwater bonding. *Underw. Technol.* **25**, 199–208 (2003).
15. Ogden, R. W. Large deformation isotropic elasticity–on the correlation of theory and experiment for incompressible rubberlike solids. *Proc. R. Soc. Lond. A Math. Phys. Sci.* **326**, 565–584 (1972).
16. Zhou, Y. et al. Instant and strong underwater adhesion by coupling hygroscopicity and in situ photocuring. *Chem. Mater.* **33**, 8822–8830 (2021).
17. Yuk, H. et al. Dry double-sided tape for adhesion of wet tissues and devices. *Nature* **575**, 169–174 (2019).
18. Liu, J. et al. Tough underwater super-tape composed of semi-interpenetrating polymer networks with a water-repelling liquid surface. *ACS Appl. Mater. Interfaces* **13**, 1535–1544 (2020).
19. Xu, Y. et al. Mussel-inspired polyesters with aliphatic pendant groups demonstrate the importance of hydrophobicity in underwater adhesion. *Adv. Mater. Interfaces* **4**, 1700506 (2017).
20. Frey, S. T. et al. Octopus-inspired adhesive skins for intelligent and rapidly switchable underwater adhesion. *Sci. Adv.* **8**, eabq1905 (2022).
21. Drotlef, D. M. et al. Insights into the adhesive mechanisms of tree frogs using artificial mimics. *Adv. Funct. Mater.* **23**, 1137–1146 (2013).
22. Lee, H. et al. Octopus-inspired smart adhesive pads for transfer printing of semiconducting nanomembranes. *Adv. Mater.* **28**, 7457–7465 (2016).
23. Baik, S. et al. A wet-tolerant adhesive patch inspired by protuberances in suction cups of octopi. *Nature* **546**, 396–400 (2017).
24. Liu, X. et al. Ingestible hydrogel device. *Nat. Commun.* **10**, 493 (2019).
25. Yuk, H., Zhang, T., Lin, S., Parada, G. A. & Zhao, X. Tough bonding of hydrogels to diverse non-porous surfaces. *Nat. Mater.* **15**, 190–196 (2016).

26. Gong, J. P. Why are double network hydrogels so tough? *Soft Matter* **6**, 2583–2590 (2010).
27. Gong, J. P., Katsuyama, Y., Kurokawa, T. & Osada, Y. Double-network hydrogels with extremely high mechanical strength. *Adv. Mater.* **15**, 1155–1158 (2003).
28. Zhang, W. et al. Fatigue of double-network hydrogels. *Eng. Fract. Mech.* **187**, 74–93 (2018).
29. Chen, J. & Shen, J. Swelling behaviors of polyacrylate superabsorbent in the mixtures of water and hydrophilic solvents. *J. Appl. Polym. Sci.* **75**, 1331–1338 (2000).
30. Zohourian, M. M. & Kabiri, K. Superabsorbent polymer materials: a review. *Iranian Polymer Journal* **17**, 451–447 (2008).
31. Ramazani-Harandi, M., Zohuriaan-Mehr, M., Yousefi, A., Ershad-Langroudi, A. & Kabiri, K. Rheological determination of the swollen gel strength of superabsorbent polymer hydrogels. *Polym. Test.* **25**, 470–474 (2006).
32. Zhang, W. et al. Factors affecting the properties of superabsorbent polymer hydrogels and methods to improve their performance: a review. *J. Mater. Sci.* **56**, 16223–16242 (2021).
33. Thorn, K. A quick guide to light microscopy in cell biology. *Mol. Biol. cell* **27**, 219–222 (2016).
34. Kováčik, J. Correlation between Young's modulus and porosity in porous materials. *J. Mater. Sci. Lett.* **18**, 1007–1010 (1999).
35. Bai, R. et al. Fatigue fracture of tough hydrogels. *Extrem. Mech. Lett.* **15**, 91–96 (2017).

Acknowledgements

We acknowledge the startup fund of the College of Engineering at Michigan State University. We acknowledge the funding support from the National Science Foundation (CMMI-2338747) and National Science Foundation (CBET-2320716).

Author contributions

J.L. and S.L. conceived the idea and designed the experiments. J.L. fabricated the sample, performed the experiments, and analyzed the results. J.L. and P.S. constructed the peeling apparatus. T.H.W. participated in the discussion. J.L. drafted the original manuscript and S.L. revised the manuscript.

Competing interests

The authors declare no competing interests.

Additional information

Supplementary information The online version contains supplementary material available at https://doi.org/10.1038/s42005-024-01921-1.

Correspondence and requests for materials should be addressed to Shaoting Lin.

Peer review information *Communications Physics* thanks Xueyu Li and the other, anonymous, reviewer(s) for their contribution to the peer review of this work. [A peer review file is available].

Reprints and permissions information is available at http://www.nature.com/reprints

Publisher's note Springer Nature remains neutral with regard to jurisdictional claims in published maps and institutional affiliations.

Open Access This article is licensed under a Creative Commons Attribution 4.0 International License, which permits use, sharing, adaptation, distribution and reproduction in any medium or format, as long as you give appropriate credit to the original author(s) and the source, provide a link to the Creative Commons licence, and indicate if changes were made. The images or other third party material in this article are included in the article's Creative Commons licence, unless indicated otherwise in a credit line to the material. If material is not included in the article's Creative Commons licence and your intended use is not permitted by statutory regulation or exceeds the permitted use, you will need to obtain permission directly from the copyright holder. To view a copy of this licence, visit http://creativecommons.org/licenses/by/4.0/.

© The Author(s) 2025